

Control of Metastable States by Heat Flux in the Hamiltonian Potts Model

Michikazu Kobayashi

*School of Environmental Science and Engineering, Kochi University of Technology,
Miyanoguchi 185, Tosayamada, Kami, Kochi 782-8502, Japan*

Naoko Nakagawa

Department of Physics, Ibaraki University, Mito 310-8512, Japan

Shin-ichi Sasa

Department of Physics, Kyoto University, Kyoto, 606-8502 Japan

(Dated: June 21, 2023)

The local equilibrium thermodynamics is a basic assumption of macroscopic descriptions of the out of equilibrium dynamics for Hamiltonian systems. We numerically analyze the Hamiltonian Potts model in two dimensions to study the violation of the assumption for phase coexistence in heat conduction. We observe that the temperature of the interface between ordered and disordered states deviates from the equilibrium transition temperature, indicating that metastable states at equilibrium are stabilized by the influence of a heat flux. We also find that the deviation is described by the formula proposed in an extended framework of the thermodynamics.

Introduction.— The macroscopic dynamics of a Hamiltonian system driven by nonequilibrium boundary conditions is expected to be described by hydrodynamic equations with local equilibrium thermodynamics [1–6]. However, there are exceptional cases, such as the shear flow near a liquid-gas critical point [7], where suppression of critical fluctuations by the shear flow modifies the thermodynamic properties [8], and as a result, the local equilibrium thermodynamics is violated. A natural question is whether the violation of the local equilibrium thermodynamics occurs except at critical points. The aim of this Letter is to provide a definitive example by studying nonequilibrium dynamics near the first-order transition point.

A first-order phase transition is a different type of singularity than the critical point [9–12]. A characteristic feature of a first-order phase transition is the existence of hysteresis [13]. For an order-disorder transition [14, 15], the observed transition temperature when a material is cooled from the disordered state is lower than the transition temperature when the same material is heated from the ordered state. Such transition temperatures, generally both in cooling and heating, deviate from the equilibrium transition temperature T_c . Thus, the supercooled disordered or the superheated ordered states are often observed as a transient dynamical process. These observations may suggest that the metastable states become steady states when the system sets up at nonequilibrium conditions. To explore this possibility, we consider steady states in heat conduction where two heat baths with temperatures T_1 and T_2 are attached at the left and right sides of the system.

We assume that T_1 and T_2 satisfy $T_1 \leq T_c \leq T_2$ to observe phase coexistence, where ordered and disordered states appear at the low and high temperature sides, respectively, with a unique interface separating the two phases. Our main question in this Letter is whether the temperature of the interface is equal to T_c . If the

local equilibrium thermodynamics is assumed to hold at each point of the system, the interface temperature should be equal to the equilibrium transition temperature. However, the validity of this assumption is not obvious because of the existence of metastable states. To our best knowledge, there have been no experimental studies on this question, while a rich variety of nonequilibrium phase-coexistence phenomena have been studied including flow boiling heat transfer and pattern formation in crystal growth [16–21].

We study the interface temperature by numerical simulations of a model that exhibits phase coexistence in steady heat conduction. Since there is no standard model for order-parameter dynamics with conducting energy, in this Letter, we propose the Hamiltonian Potts model in two dimensions. We first confirm the coexistence of ordered and disordered states in an isolated system by numerically solving the Hamiltonian equation. Then, imposing a heat flux at the boundary with the total energy fixed, we produce the phase coexistence in steady heat conduction. A remarkable property in this system is that the interface temperature deviates from the equilibrium transition temperature. This indicates that metastable states are stabilized. That is, metastability is controlled by the heat flux. Furthermore, we find that the deviation is well fitted by the formula proposed in an extended framework of thermodynamics, which we call *global thermodynamics* [22–24]. It provides a quantitative prediction of the phase coexistence in the steady heat conduction, in contrast to other extended frameworks of thermodynamics [25–32].

Model and observables.— We study the Hamiltonian Potts model with q -fold symmetry in two dimensions. Let $\phi^a(\mathbf{r})$, $a = 1, 2, \dots, q-1$, be a $q-1$ components field defined in a rectangular region $D \equiv [0, L_x] \times [0, L_y]$ with $L_x > L_y$. We express $(\phi^1, \dots, \phi^{q-1})$ as ϕ . The conjugate momentum field of $\phi^a(\mathbf{r})$ is expressed by $\pi^a(\mathbf{r})$, where π represents $(\pi^1, \dots, \pi^{q-1})$. We assume the total

Hamiltonian \mathcal{H} as

$$\mathcal{H}(\phi, \pi) = \int_D d^2\mathbf{r} \left\{ \frac{1}{2} \sum_{a=1}^{q-1} \left[(\pi^a)^2 + |\nabla\phi^a|^2 \right] + V(\phi) \right\}, \quad (1)$$

where the potential $V(\phi)$ possesses q symmetric minima in \mathbb{R}^{q-1} . Let μ_k , $1 \leq k \leq q$, be coordinates of the q vertices for the regular $(q-1)$ simplex in \mathbb{R}^{q-1} as illustrated in Fig. 1 (a) for the cases $q = 2, 3$, and 4 , where the centroid of the simplex is located at the origin. The explicit form of μ_k is given in Supplemental Material [33]. As a potential with minima at μ_k , we set

$$V(\phi) = \frac{1}{2} \prod_{k=1}^q \sum_{a=1}^{q-1} (\phi^a - \mu_k^a)^2. \quad (2)$$

This potential is regarded as a continuous extension of the standard q -state Potts model. We thus expect that the equilibrium statistical mechanics for \mathcal{H} describes the same phase transitions as those observed in the standard Potts model. As for the standard q -state Potts model, the model exhibits a first-order transition at a temperature T_c for $q \geq 5$ in equilibrium [37]. In this Letter, we numerically study the case $q = 11$ for $L_x = 384$ and $L_y = 64$. The system is spatially discretized with a grid spacing $\Delta x = 1/8$ [33]. The Boltzmann constant is set to unity.

We define the local kinetic energy density per unit degree of freedom and the local order parameter as

$$\hat{T}(\mathbf{r}) = \frac{\sum_{a=1}^{q-1} [\pi^a(\mathbf{r})]^2}{q-1}, \quad \hat{m}(\mathbf{r}) \equiv \sum_{a=1}^{q-1} \phi^a(\mathbf{r}) \mu_1^a, \quad (3)$$

where the direction of symmetry breaking is fixed to the μ_1 direction in our numerical simulations by choosing specific initial conditions [33]. Their average over the y direction with x fixed is expressed as

$$[\hat{A}]_x = \frac{1}{L_y} \int_0^{L_y} dy \hat{A}(\mathbf{r}), \quad (4)$$

where \hat{A} is \hat{T} or \hat{m} .

Equilibrium phase coexistence.— We first examine the equilibrium phase diagram by numerically investigating the isothermal dynamics [33]. The first-order transition is observed at $T = T_c \simeq 0.15$, where the energy density changes discontinuously at $T = T_c$. The system is occupied by the ordered and disordered states for $T < T_c$ and $T > T_c$, respectively. The phase diagram is shown in Fig. 1 (b).

With the knowledge of the phase diagram, we concentrate on an isolated system with the total energy E fixed. The time evolution is given by the Hamiltonian equation

$$\partial_t \phi^a = \frac{\delta \mathcal{H}}{\delta \pi^a}, \quad \partial_t \pi^a = -\frac{\delta \mathcal{H}}{\delta \phi^a}. \quad (5)$$

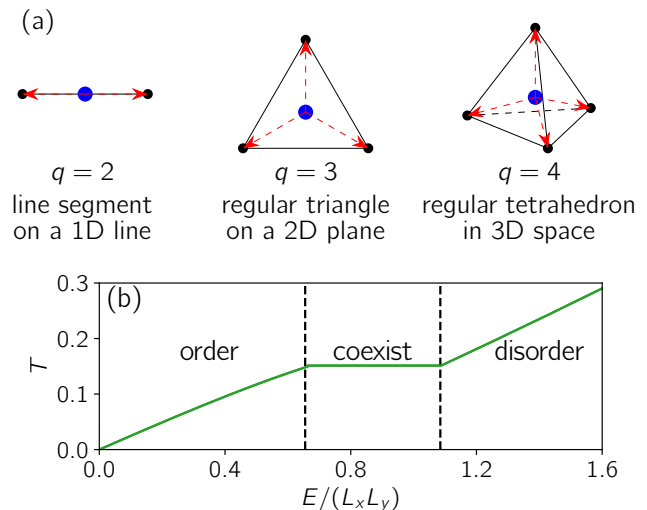


FIG. 1. (a) Examples of $(q-1)$ simplexes with q vertices in $(q-1)$ -dimensional space: a line segment with μ_1 and μ_2 for $q = 2$ (left), a regular triangle with μ_1 , μ_2 and μ_3 for $q = 3$ (middle), and a regular tetrahedron with μ_1 , μ_2 , μ_3 , and μ_4 for $q = 4$ (right). (b) Phase diagram for the $q = 11$ Hamiltonian Potts model (1). The system shows the first-order phase transition at $T = T_c$ when T is changed, while the ordered and disordered states coexist in the range $E_1 < E < E_2$. T_c , E_1 , and E_2 are numerically estimated to be $T_c \simeq 0.15$, $E_1/(L_x L_y) \simeq 0.66$, and $E_2/(L_x L_y) \simeq 1.09$ [33].

Note that

$$\frac{d\mathcal{H}}{dt} = \int_D d^2\mathbf{r} \sum_{a=1}^{q-1} \nabla \cdot (\pi^a \nabla \phi^a). \quad (6)$$

For conserving energy, we assume the Neumann boundary condition in the x direction:

$$\partial_x \phi|_{x=0, L_x} = 0 \quad (7)$$

for any y , and periodic boundary conditions in the y direction.

We start from initial conditions with a single interface and solve the Hamiltonian equation (5) until an equilibrium state is realized [33]. Figure 2(a) shows a snapshot of the local order parameter $\hat{m}(\mathbf{r})$ in equilibrium with an interface parallel to the y axis minimizing the interfacial energy. We thus discuss the one-dimensional profile by using the average over y defined by (4).

Let $\langle \hat{A} \rangle_E$ be the long-term average of $\hat{A}(\mathbf{r})$ after equilibration, which corresponds to the expected value with respect to the microcanonical distribution with E . We show the order parameter profile $m^{\text{mc}}(x) = \langle [\hat{m}]_x \rangle_E$ in Fig. 2(c), which exhibits a typical interface structure. Here, the superscript “mc” indicates “microcanonical”. The interface position X^{mc} defined as $m^{\text{mc}}(X^{\text{mc}}) = 0.5$ decreases approximately linearly with E such that $X^{\text{mc}} = L_x$ for $E = E_1$ and $X^{\text{mc}} = 0$ for $E = E_2$. There is no interface for $E < E_1$ and $E > E_2$.

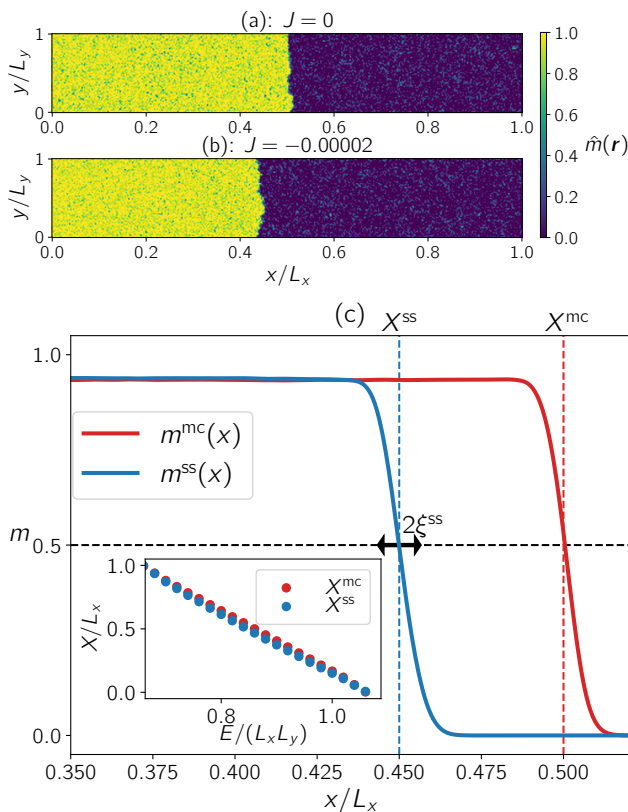


FIG. 2. (a), (b) Snapshot of the order parameter density $\hat{m}(\mathbf{r})$ in equilibrium with $J = 0$ [panel (a)] and the steady state with $J = -0.00002$ [panel (b)] for $E/(L_x L_y) = 0.88$. (c) One-dimensional order parameter profiles $m^{\text{mc}}(x)$ and $m^{\text{ss}}(x)$. The interface positions X^{mc} and X^{ss} are obtained as $m^{\text{mc}}(X^{\text{mc}}) = 0.5$ and $m^{\text{ss}}(X^{\text{ss}}) = 0.5$, respectively. The interface thickness ξ^{ss} is estimated by using $m^{\text{ss}}(x) = a - b \tanh[(x - x_0)/\xi^{\text{ss}}]$. Inset: Dependence of X^{mc} and X^{ss} on the energy density $E/(L_x L_y)$.

The one-dimensional temperature profile $T^{\text{mc}}(x) = \langle [\hat{T}]_x \rangle_E$ is homogeneous in x even for the phase coexistence observed in $E_1 < E < E_2$. This homogeneous temperature is equal to T_c obtained in isothermal systems as shown in Fig. 3 [33]. All these results show that the phase coexistence observed as an equilibrium state for the case $E \in [E_1, E_2]$ is an important feature of the isolated system and that the behavior is equivalent to the discontinuous change observed in the isothermal system, as displayed in the phase diagram in Fig. 1 (b).

Nonequilibrium phase coexistence.— We now consider phase coexistence in heat conduction. Recall that the position of the interface is uniquely determined in isolated systems for given $E \in [E_1, E_2]$, whereas it is neutral and not under control in isothermal systems at $T = T_c$. Thus, energy-conserving heat conduction could be preferable to standard heat conduction for a detailed study of thermodynamic properties. From the thermodynamic equivalence for heat conducting states as well as equilibrium states [24, 33], we expect that the obtained results

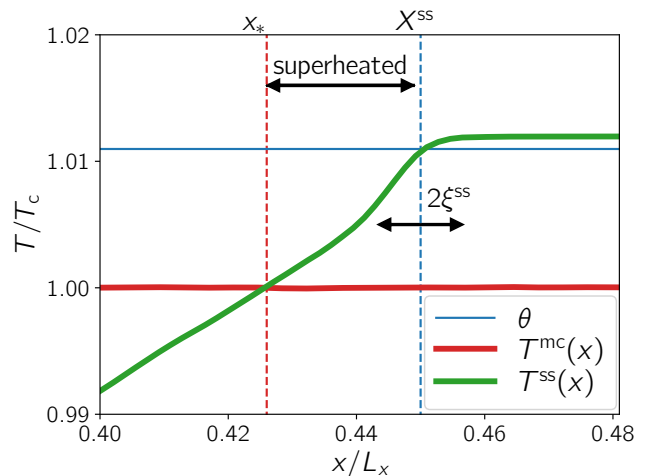


FIG. 3. One-dimensional temperature profile $T^{\text{ss}}(x)$ for $J = -0.00002$ and $T^{\text{mc}}(x)$ for $J = 0$, where $E/(L_x L_y) = 0.88$. The blue dashed line represents the interface position X^{ss} . The red dashed line represents the position x_* for $T^{\text{mc}}(x_*)$ being the equilibrium transition temperature T_c . We note that the position x_* is not at the interface region, i.e., $x_* < X^{\text{ss}} - \xi^{\text{ss}} \simeq 0.444L$.

for the energy-conserving heat-conduction systems will explain the phase coexistence observed in standard heat-conducting systems.

We construct a heat-conducting system where the energy flows in at $x = L_x$ and flows out at $x = 0$, while keeping the energy \mathcal{H} constant. That is, we impose a constant heat flux $(JL_y, 0)$ at $x = 0$ and $(JL_y, 0)$ at $x = L_x$. Recalling (6), we set

$$\partial_x \phi^a|_{x=0, L_x} = - \frac{JL_y \pi^a|_{x=0, L_x}}{\int_0^{L_y} dy \sum_{b=1}^{q-1} (\pi^b)^2|_{x=0, L_x}}, \quad (8)$$

which is a nonequilibrium generalization of (7).

We study the case $J = -0.00002$ [38]. Figure 2(b) is a snapshot of the order-parameter density field $\hat{m}(\mathbf{r})$ in the steady state, which can be compared with the equilibrium case shown in Fig. 2(a). The interface in the steady state is shifted slightly to the left of the equilibrium interface. In Fig. 2(c), we display the order-parameter profile $m^{\text{ss}}(x) = \langle [\hat{m}]_x \rangle_{E, J}$, where $\langle \cdot \rangle_{E, J}$ represents the long-term average in the steady state with E and J . For the interface position X^{ss} defined by $m^{\text{ss}}(X^{\text{ss}}) = 0.5$, we find that $|X^{\text{ss}} - X^{\text{mc}}|/L \simeq 0.05$. The inset plots X^{ss} for an energy density $E/(L_x L_y)$. The relative difference $|X^{\text{ss}} - X^{\text{mc}}|/L$ becomes smaller as E approaches E_1 or E_2 .

In Fig. 3, we plot the temperature profile $T^{\text{ss}}(x) = \langle [\hat{T}]_x \rangle_{E, J}$. An important feature is that the position x_* satisfying $T^{\text{ss}}(x_*) = T_c$ is inside the ordered regions, i.e., $x_* < X^{\text{ss}} - \xi^{\text{ss}}$, where ξ^{ss} is the interface thickness as indicated in Fig. 2(c). That is, superheated ordered states appear in a region where $T(x) > T_c$ and $m(x) > 0.5$.

This means that the local equilibrium thermodynamics is violated due to the heat flux. In other words, the temperature at the interface $\theta \equiv T^{\text{ss}}(X^{\text{ss}})$ deviates from T_c .

To study the violation more quantitatively, in Fig. 4(a), we plot θ as a function of E with $J = -0.00002$ fixed. It is notable that the interface temperature θ deviates from the equilibrium transition temperature T_c for $E \in [E_1, E_2]$. The deviation becomes a maximum around the midpoint of $[E_1, E_2]$, where the interface position is around $L_x/2$. The superheated regions disappear for $E \rightarrow E_1$ or E_2 , where the system becomes occupied by an ordered or disordered state. To examine the parameter dependence, we compare the numerical results for the violation with the formula

$$\theta^{\text{Th}} = T_c + |J| \left(\frac{1}{\kappa^{\text{o}}} - \frac{1}{\kappa^{\text{d}}} \right) \frac{X(L_x - X)}{2L_x}, \quad (9)$$

which was proposed in the global thermodynamics framework [23], where κ^{o} and κ^{d} are the heat conductivities of ordered and disordered states, respectively, and X is the position of the interface. The formula (9) can be derived for the order-disorder transition [33]. In Fig. 4(a), we simultaneously plot θ and θ^{Th} , where the latter is obtained by substituting X^{mc} into X in (9). We find that θ directly measured in numerical simulations is in qualitative agreement with θ^{Th} determined by the formula (9). The discrepancy is due to a nonlinear effect of $|J|$ as shown in the inset of Fig. 4 (a).

Finally, we investigate the finite size effects. We find that the violation of local equilibrium becomes weaker for smaller L_x or larger Δx . Instead of the original system consisting of 3073×512 grid points with $\Delta x = 1/8$, we study smaller systems consisting of 1537×256 grid points and 768×128 grid points, keeping the value of Δx fixed. The results are shown in Fig. 4 (b). The interface temperature deviates from the theoretical curve and eventually reaches the equilibrium transition temperature. This indicates that long-wavelength fluctuations play an important role in the violation of local equilibrium properties. A similar trend is observed for rough systems with larger values of Δx for the same system size. The interface temperature becomes closer to T_c as Δx increases from $1/8$ to $1/2$. This implies that regularity of the short wavelength fluctuations of the continuum fields is also necessary for the violation, which is in stark contrast to the properties in equilibrium. We do not observe the violation of local equilibrium with smaller or rougher systems. These observations suggest that hydrodynamic fluctuations on some scales play an important role for the violation of the local equilibrium at the interface.

Concluding remarks.— In this Letter, we studied nonequilibrium phase coexistence under a heat flux using the two-dimensional Hamiltonian Potts model with $q = 11$. We found that a superheated ordered region stably appears in the heat-conducting state. This indicates that the metastable states are controlled by the heat flux. Our numerical results also quantitatively sup-

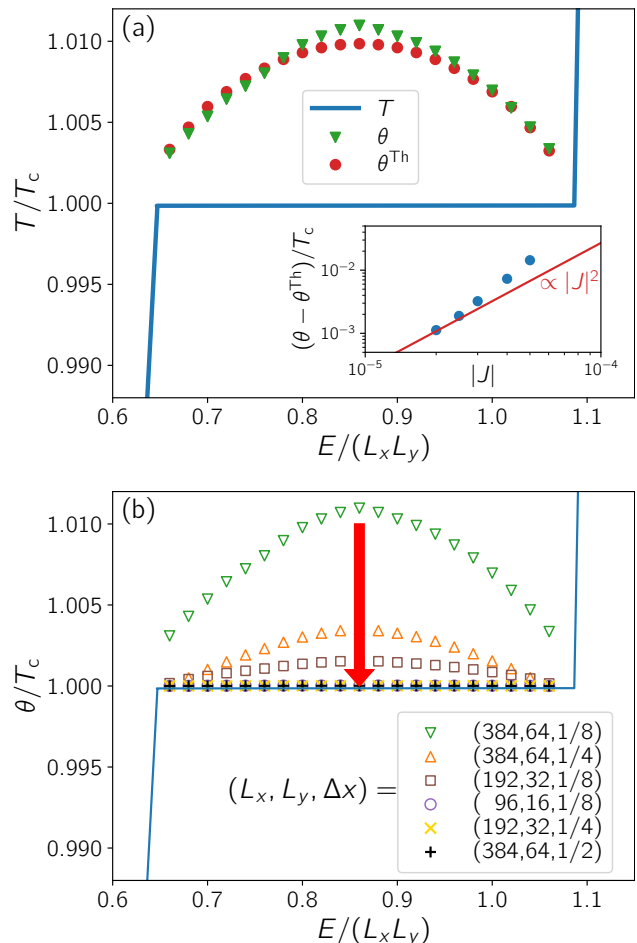


FIG. 4. (a) Interface temperature as a function of the energy density $E/(L_x L_y)$ for $J = -0.00002$. The green points are numerical values $\theta \equiv T^{\text{ss}}(X^{\text{ss}})$ and the red points are the theoretical predictions θ^{Th} in (9), substituting the numerically determined X^{mc} for X . The blue line corresponds to the green line in Fig. 1 (b). Inset: $\theta - \theta^{\text{Th}}$ are plotted for $|J|$ at $E/(L_x L_y) = 0.86$ that gives the peak value. $\theta - \theta^{\text{Th}}$ approaches the red line representing a relationship proportional to $|J|^2$. (b) Finite size effects of the numerically determined θ for $(L_x, L_y, \Delta x)$ depicted in the box with $J = -0.00002$. Several symbols are overlapped [33].

port the validity of global thermodynamics. We hope this work triggers further experimental and theoretical research, such as engineering thermodynamic metastable states. In conclusion, we present three remarks.

Although we expect that the violation of local equilibrium thermodynamics is generically observed in other models and experiments, we need to carefully choose the system conditions. For example, liquid-gas coexistence under heat conduction was studied using molecular dynamics simulations, and no violation was observed [39, 40]. We conjecture that the system sizes were too small to allow long-wavelength fluctuations that would lead to the violation of local equilibrium thermodynamics. So far, we do not estimate a crossover system size

beyond which the violation is observed. As a reference, we remark that a long-range correlation of hydrodynamic fluctuations in a sheared system is observed only when the particle number exceeds a crossover value of 10^7 [41]. We thus expect that the same order of particles are necessary for the violation. To confirm this conjecture is left for future study.

From a theoretical viewpoint, an important first study is to derive the stationary distribution of the heat conduction system. In the linear response regime, the Zubarev-McLennan representation is a generalization of the microcanonical distribution, where the correction term is expressed in terms of entropy production [3, 4], as discussed for phase coexistence in heat conduction [42]. Developing a method for estimating this correction term explicitly for microscopic or mesoscopic models is an important goal.

The most critical challenge is the observation of the violation of local equilibrium thermodynamics in laboratory experiments. As an example, for the liquid-gas coex-

istence for water at 1 atm pressure, the interface temperature was calculated to be 96°C when the temperatures of the heat baths attached to the left and right sides were 95°C and 105°C [23]. This means that super-cooled gas stably appears near the interface due to the heat flux. We believe that observation of this phenomenon is of fundamental importance.

The authors thank F. Kagawa, K. Saito, and Y. Yamamura for useful discussions on experiments of nonequilibrium phase coexistence; S. Yukawa and A. Yoshida for discussions on molecular dynamics simulations of nonequilibrium phase coexistence; and M. Itami and Y. Nakayama for discussions on fluctuating hydrodynamics. The work of M.K. was supported in part by the Osaka City University Advanced Mathematical Institute (MEXT Joint Usage/Research Center on Mathematics and Theoretical Physics, Grant No. JPMXP0619217849). The present study was supported by JSPS KAKENHI Grants No. JP19KK0066, No. JP20K03765, No. JP19K03647, No. JP19H05795, No. JP20K20425, and No. JP22H01144.

-
- [1] L. D. Landau and E. M. Lifshitz, *Fluid Mechanics* (Pergamon Press, Oxford 1959).
- [2] S. R. de Groot and P. Mazur, *Non-Equilibrium Thermodynamics* (Dover, New York, 1984).
- [3] D. N. Zubarev, *Nonequilibrium Statistical Thermodynamics* (Consultants Bureau, New York, 1974).
- [4] J. A. McLennan, Phys. Fluids **3**, 493 (1960); *Introduction to Non-Equilibrium Statistical Mechanics* (Prentice-Hall, Englewood Cliffs, 1988).
- [5] S.-i. Sasa, Derivation of Hydrodynamics from the Hamiltonian Description of Particle Systems, Phys. Rev. Lett. **112**, 100602 (2014).
- [6] T. Hayata, Y. Hidaka, T. Noumi, and M. Hongo, Relativistic hydrodynamics from quantum field theory on the basis of the generalized Gibbs ensemble method, Phys. Rev. D **92**, 065008 (2015).
- [7] A. Onuki and K. Kawasaki, Nonequilibrium steady state of critical fluids under shear flow: A renormalization group approach, Ann. Phys. (Leipzig) **121**, 456 (1979).
- [8] A. Onuki, *Phase Transition Dynamics*, (Cambridge University Press, Cambridge, 2004).
- [9] K. Binder, Theory of first-order phase transitions, Rep. Prog. Phys. **50** 783 (1987).
- [10] F. S. Bates, J. H. Rosedale, G. H. Fredrickson, and C. J. Glinka, Fluctuation-Induced First-Order Transition of an Isotropic System to a Periodic State, Phys. Rev. Lett. **61**, 2229-2232 (1988).
- [11] L. Jin, Y. Shi, F. I. Allen, L.-Q. Chen, and J. Wu, Probing the Critical Nucleus Size in the Metal-Insulator Phase Transition of VO_2 , Phys. Rev. Lett. **129**, 245701 (2022).
- [12] Q. Yang, R. Bi, D. Banerjee, and H. Nasrabad, Direct observation of the vapor-liquid phase transition and hysteresis in 2 nm Nanochannels, Langmuir **38**, 9790 (2022).
- [13] G. S. Agarwal and S. R. Shenoy, Observability of hysteresis in first-order equilibrium and nonequilibrium phase transitions, Phys. Rev. A **23** 2719 (1981).
- [14] G. L. Wang, Z. K. Qin, and D. L. Lin, First-order phase transition in order-disorder ferroelectrics, Phys. Rev. B **40**, 680 (1989).
- [15] T. Riste and L. Dobrzynski, Nematic-Isotropic Transition: Thermal Hysteresis and Magnetic Field Effects, Phys. Rev. Lett. **74**, 2737 (1995).
- [16] J. R. Thome, Boiling in microchannels: A review of experiment and theory, Int. J. Heat Fluid flow **25**, 128 (2004).
- [17] E. Ben-Jacob and P. Garik, The formation of patterns in nonequilibrium growth, Nature (London) **343**, 523 (1990).
- [18] G. Ahlers, L. I. Berge, and D. S. Cannell, Thermal Convection in the Presence of a First-Order Phase Change, Phys. Rev. Lett. **70**, 2399 (1993).
- [19] J.-Q. Zhong, D. Funfschilling, and G. Ahlers, Enhanced Heat Transport by Turbulent Two-Phase Rayleigh-Benard Convection, Phys. Rev. Lett. **102**, 124501 (2009).
- [20] S. Weiss and G. Ahlers, Nematic-isotropic phase transition in turbulent thermal convection, J. Fluid Mech. **737**, 308 (2013).
- [21] P. Urban, D. Schmoranzler, P. Hanzelka, K. R. Sreenivasan, and L. Skrbek, Anomalous heat transport and condensation in convection of cryogenic helium, Proc. Natl. Acad. Sci. U.S.A **110**, 8036 (2013).
- [22] N. Nakagawa and S.-i. Sasa, Liquid-Gas Transitions in Steady Heat Conduction, Phys. Rev. Lett. **119**, 260602 (2017).
- [23] N. Nakagawa and S.-i. Sasa, Global thermodynamics for heat conduction systems, J. Stat. Phys. **177**, 825 (2019).
- [24] N. Nakagawa and S.-i. Sasa, Unique extension of the maximum entropy principle to phase coexistence in heat conduction, Phys. Rev. Res. **4**, 033155 (2022).
- [25] J. Keizer, Thermodynamics at nonequilibrium steady states, J. Chem. Phys. **69**, 2609 (1978).
- [26] B. C. Eu, Irreversible thermodynamics of fluids, Ann. Phys. (N.Y.) **140**, 341 (1982).
- [27] D. Jou, J. Casas-Vázquez, and G. Lebon, Extended irreversible thermodynamics, Rep. Prog. Phys. **51**, 1105

- (1988).
- [28] Y. Oono and M. Paniconi, Steady state thermodynamics, *Prog. Theor. Phys. Suppl.* **130**, 29 (1998).
 - [29] S.-i. Sasa and H. Tasaki, Steady state thermodynamics, *J. Stat. Phys.* **125**, 125 (2006).
 - [30] E. Bertin, K. Martens, O. Dauchot, and M. Droz, Intensive thermodynamic parameters in nonequilibrium systems, *Phys. Rev. E* **75**, 031120 (2007).
 - [31] P. Pradhan, R. Ramsperger, and U. Seifert, Approximate thermodynamic structure for driven lattice gases in contact, *Phys. Rev. E* **84**, 041104 (2011).
 - [32] R. Dickman, Failure of steady-state thermodynamics in nonuniform driven lattice gases, *Phys. Rev. E* **90**, 062123 (2014).
 - [33] See Supplemental Material at [URL] for derivations and detailed explanations, which includes Refs. [34–36].
 - [34] B. Fornberg, *A Practical Guide to Pseudospectral Methods* (Cambridge University Press, Cambridge, England, 1995).
 - [35] R. I. McLachlan and G. R. W. Quispel, Splitting methods, *Acta Numer.* **11**, 341 (2002).
 - [36] M. Ohzeki and A. Ichiki, Langevin dynamics neglecting detailed balance condition, *Phys. Rev. E* **92**, 012105 (2015).
 - [37] F. Y. Wu, The Potts model, *Rev. Mod. Phys.* **54** 235 (1982).
 - [38] This value was chosen so that the system is in the linear response regime in J . For example, linear temperature profiles are observed in the ordered and disordered phases [33].
 - [39] A. Røsjorde, D. W. Fossmo, D. Bedeaux, S. Kjelstrup, and B. Hafskjold, Nonequilibrium molecular dynamics simulations of steady-state heat and mass transport in condensation: I. Local equilibrium, *J. Coll. Int. Sci.* **232**, 178 (2000).
 - [40] S. Yukawa (private communication).
 - [41] H. Nakano and Y. Minami, Molecular dynamics study of shear-induced long-range correlations in simple fluids, *Phys. Rev. Res.* **4**, 023147 (2022).
 - [42] S.-i. Sasa, N. Nakagawa, M. Itami, and Y. Nakayama, Stochastic order parameter dynamics for phase coexistence in heat conduction, *Phys. Rev. E* **103**, 062129 (2021).

Supplemental Material for “Control of metastable states by heat flux in the Hamiltonian Potts model”

Michikazu Kobayashi¹, Naoko Nakagawa², and Shin-ichi Sasa³

¹*School of Environmental Science and Engineering, Kochi University of Technology, Miyanoguchi 185, Tosayamada, Kami, Kochi 782-8502, Japan*

²*Department of Physics, Ibaraki University, Mito 310-8512, Japan*

³*Department of Physics, Kyoto University, Kyoto, 606-8502 Japan*

This Supplemental Material consists of three sections. In Sec. I, we review global thermodynamics for the system we study. The goal of this section is to derive the formula (9) in the main text. In Sec. II, we present details of numerical simulations of the Hamiltonian equation (5) to support the results of the main text. In Sec. III, we explain the isothermal dynamics by which the equilibrium phase diagram for the temperature is determined.

I. GLOBAL THERMODYNAMICS

First of all, we introduce an external field $H \geq 0$ for formulating thermodynamics of ordered and disordered states. While the numerical computation in the main text was performed without imposing any external field, we study a spontaneous symmetry-breaking state by considering the limit $H \rightarrow 0^+$.

To set up the system, we notice the order parameter field $\hat{m}(\mathbf{r})$ defined as (3) and introduce a uniform field H acting on $\hat{m}(\mathbf{r})$ by assuming the Hamiltonian of the system as

$$\mathcal{H}(\phi, \pi) - H\hat{M}(\phi). \quad (\text{S.1})$$

The Hamiltonian \mathcal{H} without the external field is defined in (1) and the total order parameter \hat{M} is defined as the spatial integration

$$\hat{M} = \int d^2\mathbf{r} \hat{m}(\mathbf{r}). \quad (\text{S.2})$$

We assume that thermodynamic properties are not qualitatively changed by applying the external field for sufficiently small H . For instance, the equilibrium transition temperature may continuously change with H , which we write $T_c(H)$. Below $T_c(H)$ the ordered phase appears as studied in the main text. From the symmetry, $T_c(H) = T_c(0) + O(H^2)$.

In Sec. IA, we briefly review equilibrium thermodynamics. In Sec. IB, we formulate global thermodynamics for the bulk of ordered and disordered states in steady heat conduction. In Sec. IC, we present the variational principle for determining the steady phase coexistence state in heat conduction. Section ID is devoted to the derivation of (9) used in the main text. In Sec. IE, we explain the thermodynamic relations in heat conduction and the equivalence of steady states of the energy-conserved system with the system conducted by two heat baths.

A. Equilibrium thermodynamics

We review equilibrium thermodynamics for the model we study in the main text.

In the thermodynamic limit, \mathcal{H} and \hat{M} form the internal energy U and macroscopic order parameter M . Letting E be the total energy of the system, (S.1) leads to $E = U - HM$. Changing the value of H to $H + dH$ requires work $d'W = -MdH$. Since $d'Q = TdS$, the energy conservation forms the first law of thermodynamics as

$$dE = TdS - MdH. \quad (\text{S.3})$$

Thus, the entropy S is given as a function of (E, H) for a fixed volume of the system $V = L_x L_y$ with the relation

$$dS = \frac{dE}{T} + \frac{M}{T}dH. \quad (\text{S.4})$$

Since $S(E, H, V)$ satisfies the extensivity

$$S(\lambda E, H, \lambda V) = \lambda S(E, H, V) \quad (\text{S.5})$$

for any $\lambda > 0$, we can derive

$$dS = \frac{dE}{T} + \frac{M}{T}dH - \frac{f}{T}dV \quad (\text{S.6})$$

with $f = (E - TS)/V$ which corresponds to the free-energy density. Since we study the case $H = 0$ in the main text, the internal energy U is equal to the total energy E .

B. Heat conduction without phase coexistence

Next, we study the linear response regime in heat conduction systems without phase coexistence. Specifically, we consider the case that the heat flux is in parallel to the x -axis for simplicity. We then assume the existence of local thermodynamic quantities $a(\mathbf{r})$, which are independent of y . We express them as $a(x)$ simply. The arguments below follow Sec. 3 of ref. [1].

Let $s(x)$, $T(x)$, $e(x)$, and $m(x)$ be local entropy density, local temperature, local energy density, and local order parameter density. These local quantities satisfy the fundamental relation,

$$ds(x) = \frac{de(x)}{T(x)} + \frac{m(x)}{T(x)}dH, \quad (\text{S.7})$$

for each x . The total amounts of extensive quantities in heat conduction are obtained by the integration of corresponding local quantities such that

$$S = L_y \int_0^{L_x} dx s(x), \quad E = L_y \int_0^{L_x} dx e(x), \quad M = L_y \int_0^{L_x} dx m(x). \quad (\text{S.8})$$

Hereafter, we call these ‘‘global thermodynamic quantities.’’ We then define a global temperature and a global free energy density to characterize the heat conduction states as the mean value of the respective local values as

$$\tilde{T} = \frac{1}{L_x} \int_0^{L_x} dx T(x), \quad (\text{S.9})$$

$$\tilde{f} = \frac{1}{L_x} \int_0^{L_x} dx f(x). \quad (\text{S.10})$$

In the linear response regime, the quantities defined by the spatial integration such as (S.8), (S.9) and (S.10) are estimated by the trapezoidal rule. Thus the global quantities are represented by corresponding local thermodynamic quantities at the midpoint $x = L_x/2$. This indicates that the nonequilibrium entropy in (S.8) is approximated by the equilibrium entropy function; i.e.,

$$S = S(E, H, V) + O(\varepsilon^2), \quad (\text{S.11})$$

where ε is a dimensionless small parameter proportional to J . Straightforwardly, the global thermodynamic quantities in heat conduction satisfy the fundamental relation of thermodynamics

$$dS = \frac{dE}{\tilde{T}} + \frac{M}{\tilde{T}}dH - \frac{\tilde{f}}{\tilde{T}}dV, \quad (\text{S.12})$$

with an error of $O(\varepsilon^2)$. While global quantities E , M , and V are naturally defined for the heat conduction states, \tilde{T} and \tilde{f} are given as nonequilibrium extensions of the temperature and the free energy density through the thermodynamic relation (S.12).

C. Phase coexistence in heat conduction

Let us concentrate on the energy-conserving heat-conduction system. Choosing the value of E in a certain range, say $[E_1, E_2]$, we observe the phase coexistence with a planar interface. In equilibrium, the temperature at the phase coexistence is kept at the transition temperature $T_c(H)$. Now, we impose the energy flux J in such a way that the total energy E is conserved, where $J < 0$ is assumed without loss of generality. We then observe the phase coexistence of the ordered state in $0 \leq x \leq X$ and the disordered state in $X \leq x \leq L_x$, where X is to the interface position. The temperature field $T(x)$ and the order parameter field $m(x)$ satisfy the local thermodynamic relation in each phase, while there is no established law for determining the interface temperature θ . Here, let us recall that the equilibrium state in the phase coexistence for given (E, H, V) is determined by the maximum entropy principle, where the equilibrium state maximizes the total entropy. We extend this variational principle to that for heat conduction states.

We start with global thermodynamics in each region introduced in Sec. IB. The global entropies are expressed as

$$S^o = S(E^o, H, L_y X), \quad S^d = S(E^d, H, L_y(L_x - X)), \quad (\text{S.13})$$

where we put the superscript “o” or “d” to indicate the quantities in the ordered or disordered phase. From the fundamental relation (S.12), we have

$$\left(\frac{\partial S^{\circ}}{\partial E^{\circ}}\right)_{H,X} = \frac{1}{\tilde{T}^{\circ}}, \quad \left(\frac{\partial S^{\text{d}}}{\partial E^{\text{d}}}\right)_{H,L-X} = \frac{1}{\tilde{T}^{\text{d}}}, \quad (\text{S.14})$$

$$\frac{1}{L_y} \left(\frac{\partial S^{\circ}}{\partial X}\right)_{E^{\circ},H} = -\frac{\tilde{f}^{\circ}}{\tilde{T}^{\circ}}, \quad \frac{1}{L_y} \left(\frac{\partial S^{\text{d}}}{\partial(L_x - X)}\right)_{E^{\text{d}},H} = -\frac{\tilde{f}^{\text{d}}}{\tilde{T}^{\text{d}}}. \quad (\text{S.15})$$

Letting $T_1 = T(0)$, $T_2 = T(L)$, and $\theta = T(X)$, the trapezoidal rule yields

$$\tilde{T}^{\circ} = \frac{T_1 + \theta}{2}, \quad \tilde{T}^{\text{d}} = \frac{T_2 + \theta}{2}. \quad (\text{S.16})$$

Note that θ is the interface temperature. T_1 and T_2 are temperatures at the left and right boundaries of the system, respectively.

For determining steady states in phase coexistence, thermodynamics provides variational principles. For the equilibrium case $J = 0$, the equilibrium state with E , H , and V fixed maximizes the total entropy $S = S^{\circ} + S^{\text{d}}$ with respect to E° and X . Here, E is the total amount of energy of the system and $E^{\text{d}} = E - E^{\circ}$. The variational equations lead to $\tilde{T}^{\circ} = \tilde{T}^{\text{d}}$ and $\tilde{f}^{\circ} = \tilde{f}^{\text{d}}$. For heat conduction cases $J < 0$, as derived in [2], the entropy as the variational function is concluded as

$$S = S^{\circ} + S^{\text{d}} + \phi\Psi \quad (\text{S.17})$$

with

$$\phi = \frac{T_2 - T_1}{T_c(H)}, \quad (\text{S.18})$$

$$\Psi = \frac{E^{\text{d}}X - E^{\circ}(L_x - X)}{2T_c(H)L_x}. \quad (\text{S.19})$$

The steady state with E , H , L_x , and ϕ fixed is determined as the state maximizing (S.17) with respect to E° and X . We then obtain the condition for the steady state as

$$\tilde{T}^{\text{d}} - \tilde{T}^{\circ} = \frac{\phi T_c(H)}{2}, \quad (\text{S.20})$$

$$\frac{\tilde{f}^{\circ}}{\tilde{T}^{\circ}} - \frac{\tilde{f}^{\text{d}}}{\tilde{T}^{\text{d}}} = \phi \frac{E}{2T_c(H)L_xL_y}. \quad (\text{S.21})$$

Note that these two relations are the extension of the equilibrium balance relations $\tilde{T}^{\circ} = \tilde{T}^{\text{d}}$ and $\tilde{f}^{\circ} = \tilde{f}^{\text{d}}$. Due to the nonequilibrium contributions in the right-hand sides of (S.20) and (S.21), we find that the steady states contain metastable states in a region adjacent to the interface. See (9) and its derivation in Sec. ID.

D. Derivation of (9)

For simplicity of the derivation below, we introduce $\alpha \equiv -f/T$. Since $\alpha = s - e/T$, the equilibrium fundamental relation (S.7) yields

$$d\alpha = \frac{e}{T^2}dT + \frac{m}{T}dH. \quad (\text{S.22})$$

We also notice $E = E^{\circ} + E^{\text{d}}$, $E^{\circ} = e_c^{\circ}XL_y + O(\varepsilon)$, and $E^{\text{d}} = e_c^{\text{d}}(L_x - X)L_y + O(\varepsilon)$ with $e_c^{\circ/\text{d}} \equiv e^{\circ/\text{d}}(T_c(H), H)$. Using α and these relations, (S.21) is written as

$$\tilde{\alpha}^{\text{d}} - \tilde{\alpha}^{\circ} = \frac{\phi}{2T_c(H)} \left(e_c^{\circ} \frac{X}{L_x} + e_c^{\text{d}} \frac{L_x - X}{L_x} \right) + O(\varepsilon^2). \quad (\text{S.23})$$

Since $\tilde{\alpha}^{\circ/\text{d}} = \alpha^{\circ/\text{d}}(\tilde{T}^{\circ/\text{d}}, H)$ with the equilibrium functions $\alpha^{\circ/\text{d}}(T, H)$, we have

$$\tilde{\alpha}^{\text{d}} - \tilde{\alpha}^{\circ} = \alpha^{\text{d}}(T_c(H), H) + \frac{e_c^{\text{d}}}{T_c(H)^2}(\tilde{T}^{\text{d}} - T_c(H)) - \alpha^{\circ}(T_c(H), H) - \frac{e_c^{\circ}}{T_c(H)^2}(\tilde{T}^{\circ} - T_c(H)) + O(\varepsilon^2). \quad (\text{S.24})$$

Substituting this into (S.23) and using the equilibrium balance $\alpha^o(T_c(H), H) = \alpha^d(T_c(H), H)$, we obtain

$$e_c^o \left(\tilde{T}^o - T_c(H) + \frac{\phi T_c(H) X}{2 L_x} \right) - e_c^d \left(\tilde{T}^d - T_c(H) - \frac{\phi T_c(H) L_x - X}{2 L_x} \right) = 0. \quad (\text{S.25})$$

The global temperature \tilde{T} for the phase coexistence, which is defined by (S.9), is expressed as

$$\tilde{T} = \tilde{T}^o \frac{X}{L_x} + \tilde{T}^d \frac{L_x - X}{L_x}. \quad (\text{S.26})$$

Combining this with (S.20), we have

$$\tilde{T}^o = \tilde{T} - \frac{\phi T_c(H) L_x - X}{2 L_x}, \quad \tilde{T}^d = \tilde{T} + \frac{\phi T_c(H) X}{2 L_x}, \quad (\text{S.27})$$

where we have used $\tilde{T} = T_c(H) + O(\varepsilon)$. Substituting (S.27) into (S.25), we obtain

$$(e_c^d - e_c^o) \left(\tilde{T} - T_c(H) - \frac{\phi T_c(H) L_x - 2X}{2 L_x} \right) = 0. \quad (\text{S.28})$$

Note that $e_c^d - e_c^o \neq 0$ in the first-order transition. The relation (S.28) together with (S.27) leads to

$$\tilde{T}^o = T_c(H) - \frac{\phi T_c(H) X}{2 L_x}, \quad \tilde{T}^d = T_c(H) + \frac{\phi T_c(H) L_x - X}{2 L_x}. \quad (\text{S.29})$$

Applying (S.16), the first relation of (S.29) is rewritten as

$$T_1 = 2T_c(H) - \theta - \phi T_c(H) \frac{X}{L_x}. \quad (\text{S.30})$$

Finally, let us recall that the heat flux is uniform in x from the conservation of energy, which is expressed as

$$J = -\kappa^o \frac{\theta - T_1}{X} = -\kappa^d \frac{T_2 - \theta}{L_x - X}, \quad (\text{S.31})$$

where $\kappa^{o/d}$ is the heat conductivity at the transition temperature, $\kappa^{o/d} = \kappa^{o/d}(T_c(H), H)$. (S.31) is transformed to

$$T_1 = \theta + J \frac{X}{\kappa^o}, \quad (\text{S.32})$$

$$\phi = -\frac{J}{T_c} \left(\frac{X}{\kappa^o} + \frac{L_x - X}{\kappa^d} \right). \quad (\text{S.33})$$

We now substitute these two relations into (S.30). We then obtain

$$\theta = T_c(H) - J \left(\frac{1}{\kappa^o} - \frac{1}{\kappa^d} \right) \frac{X(L_x - X)}{2L_x}. \quad (\text{S.34})$$

To this point, we have assumed $J < 0$. Repeating the same argument for the case $J > 0$, we find that θ is symmetric for the transformation $J \rightarrow -J$. We thus conclude (9).

E. Thermodynamic relations in phase coexistence

Thermodynamic entropy corresponds to the maximum value of the variational function (S.17). With ϕ and Ψ given in (S.18) and (S.19), and applying the variational equations (S.20) and (S.21), we have the fundamental relation of global thermodynamics as [2]

$$dS = \frac{dE}{\tilde{T}} + \frac{M}{\tilde{T}} dH - \frac{\tilde{f}}{\tilde{T}} dV + \Psi d\phi. \quad (\text{S.35})$$

Thus, the global entropy is $S = S(E, H, V, \phi)$, i.e., a different function from the equilibrium entropy.

As a more familiar setup for heat conduction, one may consider a system between two heat baths of T_1 and T_2 . Since the total energy E is not conserved, natural thermodynamic variables would be (\tilde{T}, H, V, ϕ) considering a straightforward extension from that for equilibrium systems with a heat bath. Here the global temperature \tilde{T} is defined by (S.9) and connected to the global temperatures in the ordered and disordered regions as

$$\tilde{T} = \frac{X}{L_x} \tilde{T}^o + \frac{L_x - X}{L_x} \tilde{T}^d. \quad (\text{S.36})$$

We can show the equivalence of the steady state in heat conduction between such systems and the energy-conserved systems investigated in the main text. More precisely, (9) results from the minimization of a variational function corresponding to the spatial integration of free energy $F = L_y \int_0^{L_x} f(x) dx$. It is written as $F = F^o + F^d$ with $F^o = F(\tilde{T}^o, H, L_y X)$ and $F^d = F(\tilde{T}^d, H, L_y(L_x - X))$, and the minimum value of F satisfies a thermodynamic relation

$$dF = -Sd\tilde{T} - MdH + \tilde{f}dV - \tilde{T}\Psi d\phi, \quad (\text{S.37})$$

which indicates the nonequilibrium free energy is written as $F = F(\tilde{T}, H, V, \phi)$. The two fundamental relations (S.35) and (S.37) are connected by the Legendre transformation with

$$F = E - \tilde{T}S + O(\varepsilon^2), \quad (\text{S.38})$$

which is led from the spatial integration of the local thermodynamic relation

$$f(x) = e(x) - T(x)s(x) \quad (\text{S.39})$$

using \tilde{T} in (S.36) and the entropy in (S.17).

II. DETAILS OF NUMERICAL SIMULATIONS

A. Explicit form for μ_k of (2)

We explicitly derive coordinates μ_k^a ($1 \leq k \leq q$, $1 \leq a \leq q-1$) of the q vertex for the regular $(q-1)$ simplex in \mathbb{R}^{q-1} . We first notice that μ_k^a should satisfy the following three conditions:

(i) the centroid is located at the origin:

$$\sum_{k=1}^q \mu_k^a = 0, \quad (\text{S.40})$$

(ii) the length between the centroid and each vertex is one:

$$\sum_{a=1}^{q-1} (\mu_k^a)^2 = 1, \quad (\text{S.41})$$

(iii) the length between two different vertices is constant:

$$\sum_{a=1}^{q-1} (\mu_k^a - \mu_{k'}^a)^2 = K(1 - \delta_{kk'}) \quad (\text{S.42})$$

for any $1 \leq k, k' \leq q$, where K is a constant. We then find that (S.40), (S.41), and (S.42) are satisfied by

$$\mu_k^a = \begin{cases} \frac{\sqrt{q}}{\sqrt{q-1}} \delta_k^a - \frac{\sqrt{q}+1}{(q-1)^{3/2}}, & 1 \leq k \leq q-1, \\ \frac{1}{\sqrt{q-1}}, & k = q, \end{cases} \quad (\text{S.43})$$

with $K = 2q/(q-1)$.

B. Numerical simulations of the Hamiltonian equation (5) with the boundary condition (7)

We numerically solve the Hamiltonian equation (5). By imposing the boundary condition (7), the system conserves the total amount of energy E . Hereafter, we consider only the case with odd q .

First, we discretize a box of $(L_x, L_y) = (384, 64)$ with a lattice spacing length $\Delta x = 1/8$ in both x and y directions. Then the system consists of $N_x \times N_y$ grid points, i.e., $(N_x, N_y) = (3073, 512)$. To calculate the spatial derivative $\nabla^2 \phi^a$ included in $\delta\mathcal{H}/\delta\phi^a$, we use the following spectral collocation method [3]. We first construct $(q-1)/2$ -complex fields

$$\Phi^a = \phi^{2a-1} + i\phi^{2a} \quad (\text{S.44})$$

from $(q-1)$ -real fields ϕ^a , where $1 \leq a \leq (q-1)/2$. We evaluate the spatial derivative $\nabla^2 \Phi^a = \nabla^2 \phi^{2a-1} + i\nabla^2 \phi^{2a}$ by the Fourier transformation

$$\begin{aligned} \nabla^2 \Phi^a(x, y, t) &= -\frac{1}{(N_x-1)N_y} \sum'_{n_x=0}^{N_x-1} \sum_{n_y=-N_y/2+1}^{N_y/2} (k_x^2 + k_y^2) \tilde{\Phi}^a(n_x, n_y, t) \cos(k_x x) e^{ik_y y}, \\ k_x &= \frac{\pi n_x}{L_x}, \quad k_y = \frac{2\pi n_y}{L_y}, \end{aligned} \quad (\text{S.45})$$

where we define

$$\sum'_{n=n_i}^{n_f} f(n) \equiv \frac{f(n_i) + f(n_f)}{2} + \sum_{n=n_i+1}^{n_f-1} f(n). \quad (\text{S.46})$$

The Fourier basis functions in (S.45) are cosine functions in x direction to satisfy the boundary condition (7). The Fourier component $\tilde{\Phi}^a(n_x, n_y, t)$ in (S.45) is obtained by the inverse transformation

$$\tilde{\Phi}^a(n_x, n_y, t) = 2 \sum'_{I=0}^{N_x-1} \sum_{J=0}^{N_y-1} \Phi^a(x, y, t) \cos(k_x I \Delta x) e^{-ik_y J \Delta x}, \quad (\text{S.47})$$

where Δx is the lattice spacing length. The variables Φ defined on the $N_x \times N_y$ grid points evolve according to the Hamiltonian equation (5). To obtain the time evolution of them, we adopt the 4th-order Strang splitting (symplectic integrator) method [4] with the temporal interval $\Delta t = 1/4096$. We confirmed that the energy is conserved as $|\langle \mathcal{H} \rangle_t - \langle \mathcal{H} \rangle_{t=0}| / \langle \mathcal{H} \rangle_{t=0} < 10^{-8}$.

We denote the solution of the Hamiltonian equation (5) with the boundary condition (7) as $(\phi, \pi)_E(\mathbf{r}, t)$, where E is the amount of the energy (the value of \mathcal{H}), which is determined by the initial condition and conserved in the time evolution. Aiming at observing the phase coexistence of the ordered and disordered states, we set the initial condition as a connected configuration of two equilibrium configurations prepared at different temperatures:

$$(\phi, \pi)_E(x, y, 0) = \begin{cases} (\phi_1, \pi_1)_{T_1}(x, y, t_f) & 0 \leq x < L_x/2, \\ (\phi_1, \pi_1)_{T_2}(x - L_x/2, y, t_f) & L_x/2 \leq x < L_x, \\ (\phi_1, \pi_1)_{T_2}(0, y, t_f) & x = L_x, \end{cases} \quad (\text{S.48})$$

where $(\phi_1, \pi_1)_T$ is the solution of (S.71) with the isothermal condition at T , which will be explained in Sec. III. Thus, the energy E is determined depending on the chosen initial condition with T_1 and T_2 . We fix $T_1 = 0.63T_c$, and change T_2 from $0.63T_c$ to $2.0T_c$. Accordingly, the energy E changes from $E/(L_x L_y) = 0.5$ to $E/(L_x L_y) = 1.2$.

Figure S.1 (a) shows an example of the time evolution of the one-dimensional order-parameter profile $[\hat{m}]_x$ as a function of t . We see that the interface shifts from the initial position and relax to an equilibrium position. We expect that the interface dynamics is the slowest in the equilibration process. Then, we estimate the relaxation time t_* of the interface as follows. Let the interface position \hat{X} be the value of x satisfying $[\hat{m}]_x = 0.5$. When there are several values of x satisfying $[\hat{m}]_x = 0.5$, we choose \hat{X} as their centroid. In Fig. S.1 (b), we show the t -dependence of \hat{X} . We define the relaxation time t_* by using a functional form $\hat{X} \simeq X_0(1 - \alpha e^{-t/t_*})$ in the range $0.5 \times 10^6 \leq t \leq 2.0 \times 10^6$. We obtain $t_* \simeq 5.3 \times 10^5$. Based on the result, we define the long-term average of $\hat{A}(\mathbf{r}, t)$ as

$$\langle \hat{A}(\mathbf{r}) \rangle_E \equiv \frac{1}{t_f - t_0} \int_{t_0}^{t_f} dt \hat{A}(\mathbf{r}, t), \quad (\text{S.49})$$

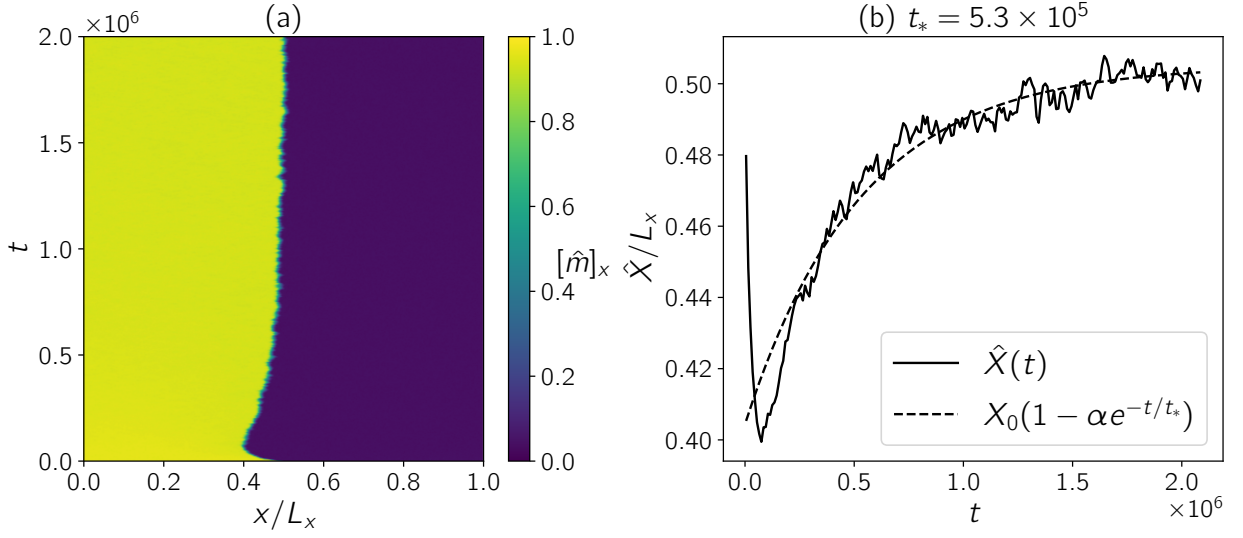


FIG. S.1. (a) Time evolution of the averaged order parameter density $[\hat{m}]_x$ according to the Hamiltonian equation (5) with the boundary condition (7). The initial condition is given by a combination of two equilibrium snapshots with different temperatures $T_1 = 0.63T_c$ (left region) and $T_2 = 1.1T_c$ (right region). (b) Dependence of the interface position \hat{X} on time t . The dashed lines show the fitting with $X_0(1 - \alpha e^{-t/t_*})$ for $\hat{X}(t)$. The energy density is set to $E/(L_x L_y) = 0.88$.

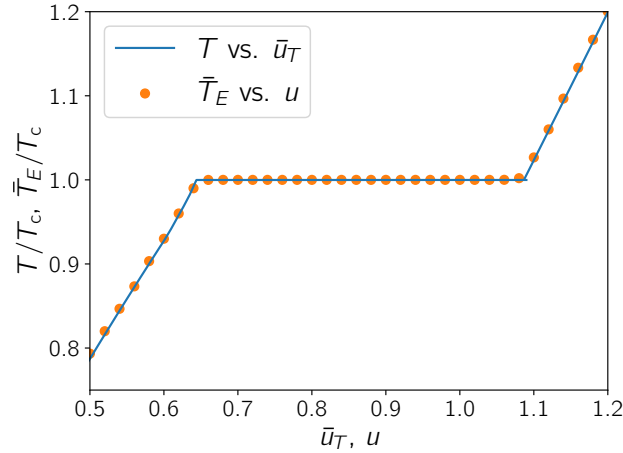


FIG. S.2. (Orange dots) microcanonical temperature \bar{T}_E as a function of energy density $u = E/(L_x L_y)$. (Blue line) canonical energy density \bar{u}_T as a function of temperature T . T_c is the transition temperature determined from the canonical simulations.

where we set $t_0 = 2 \times 10^6$ and $t_f = t_0 + 3.2 \times 10^4$. Note that $t_0 \simeq 4t_*$, which would be sufficient for equilibration as shown in Fig. S.1 (b). We thus conjecture that $\langle \hat{A}(\mathbf{r}) \rangle_E$ is approximately equal to the expected value of $\hat{A}(\mathbf{r})$ with respect to the microcanonical ensemble

$$\rho_E^{\text{mc}}(\phi, \pi) = \frac{1}{\Sigma} \delta(E - \mathcal{H}(\phi, \pi)), \quad (\text{S.50})$$

where Σ is the normalization constant.

In Fig. S.2, we show the numerical results of the microcanonical temperature \bar{T}_E given by

$$\bar{T}_E = \frac{1}{L_x L_y} \int_D d^2 \mathbf{r} \langle \hat{T}(\mathbf{r}) \rangle_E, \quad \hat{T}(\mathbf{r}) = \frac{\sum_{a=1}^{q-1} (\pi^a(\mathbf{r}))^2}{2(q-1)} \quad (\text{S.51})$$

as a function of the energy density $u = E/(L_x L_y)$. We observe a plateau in a range $0.66 \lesssim u \lesssim 1.09$, which indicates the realization of the phase coexistence. We also find good agreement of the data (u, \bar{T}_E) with another data (\bar{u}_T, T) , where \bar{u}_T is the energy density of an isothermal system with the temperature T . See Sec. III for numerical simulations of the isothermal system.

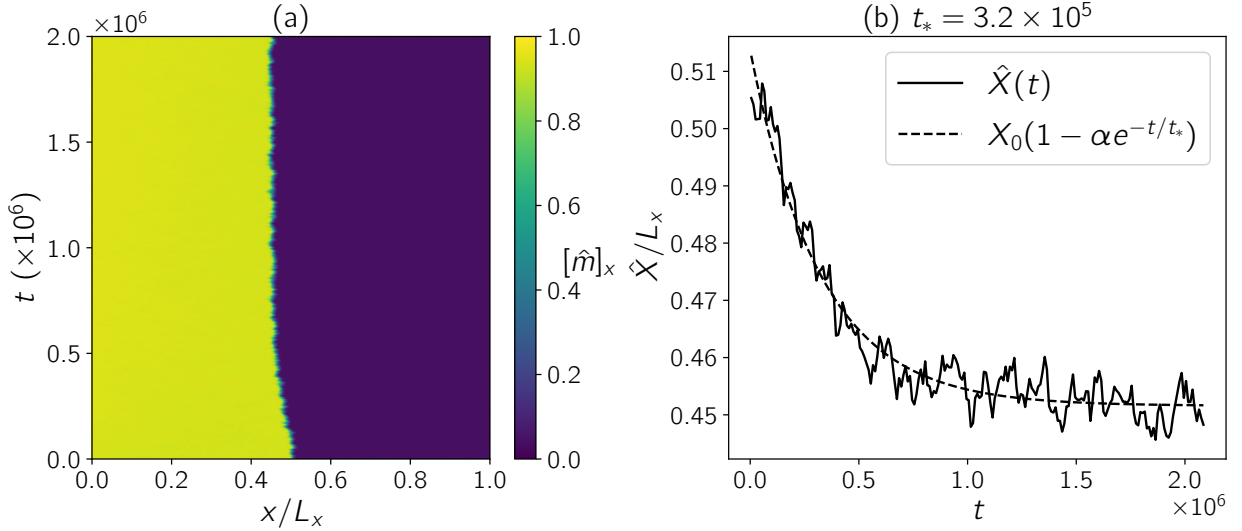


FIG. S.3. (a) Time evolution of the averaged order parameter density $[\hat{m}]_x$ in the nonequilibrium dynamics under the heat conduction. (b) Dependence of the interface position \hat{X} on the time t . The dashed lines show the fitting with $X_0(1 - \alpha e^{-t/t_*})$ for $\hat{X}(t)$. The energy density is set to $E/(L_x L_y) = 0.88$.

C. Numerical simulations of the Hamiltonian equation (5) with the boundary condition (8)

To study the system under the constant heat flux $(JL_y, 0)$, we solve the Hamiltonian equation (5) with the nonequilibrium boundary condition (8). Since the evolution equation (5) is unchanged from the previous section, we apply the same numerical methods, i.e., spectral collocation and 4-th order Strang splitting methods. The only difference from Sec. II B is the boundary condition, which is changed from (7) to (8). To apply (8), letting $B_{x=0, L_x}$ be the right-hand side in (8), (S.45) should be modified as

$$\nabla^2 \Phi^a(x, y, t) = \frac{B_L^a - B_0^a}{L_x} - \frac{1}{(N_x - 1)N_y} \sum_{n_x=0}^{N_x-1} \sum_{n_y=-N_y/2+1}^{N_y/2} (k_x^2 + k_y^2) \tilde{\Phi}^a(n_x, n_y, t) \cos(k_x x) e^{ik_y y}, \quad (\text{S.52})$$

where $B_{x=0, L_x}^a$ is explicitly expressed as

$$B_{x=0, L_x}^a \equiv - \frac{JL_y \Pi^a|_{x=0, L_x}}{\int_0^{L_y} dy \sum_{b=1}^{q-1} \Pi^{b*} \Pi^b|_{x=0, L_x}}, \quad \Pi^a \equiv \pi^{2a-1} + i\pi^{2a}. \quad (\text{S.53})$$

Accordingly, the Fourier component $\tilde{\Phi}^a(n_x, n_y, t)$ in (S.45) is replaced by

$$\tilde{\Phi}^a(n_x, n_y, t) = 2 \sum_{I=0}^{N_x-1} \sum_{J=0}^{N_y-1} \left\{ \Phi^a(x, y, t) - B_0^a - \frac{(B_L^a - B_0^a)(I\Delta x)^2}{2L} \right\} \cos(k_x I\Delta x) e^{-ik_y J\Delta x}. \quad (\text{S.54})$$

We denote the solution of the Hamiltonian equation (5) with the boundary condition (8) as $(\phi, \pi)_{E, J}(\mathbf{r}, t)$. We then confirmed that the energy is conserved as $|\langle \mathcal{H} \rangle_t - \langle \mathcal{H} \rangle_{t=0}| / \langle \mathcal{H} \rangle_{t=0} < 10^{-8}$.

To observe the effect of the heat flux clearly, we set the initial condition as the final state of the equilibrium simulations performed in the previous section: $(\phi, \pi)_{E, J}(\mathbf{r}, 0) = (\phi, \pi)_E(\mathbf{r}, t_f)$. Figure S.3 (a) shows an example of the dynamics for the one-dimensional order-parameter profile $[\hat{m}]_x$. We see that the interface slowly shifts from the initial equilibrium position corresponding to the final position in Fig. S.1 (a). This clearly shows that the heat flux changes the steady state. The relaxation dynamics seems similar to the equilibrium one. Then, we estimate the equilibrating time t_* of the interface in Fig. S.3 (b) with using the interface position \hat{X} . By fitting \hat{X} in the range $0 \leq t \leq t_0 = 2.0 \times 10^6$, we obtain $t_* \simeq 3.2 \times 10^5$. Thus, we expect that the system reaches the nonequilibrium steady state before t_0 and regard the expected value $\langle \hat{A}(\mathbf{r}) \rangle_{E, J}$ in the steady state as

$$\langle \hat{A}(\mathbf{r}) \rangle_{E, J} \equiv \frac{1}{t_f - t_0} \int_{t_0}^{t_f} dt \hat{A}(\mathbf{r}, t) \quad (\text{S.55})$$

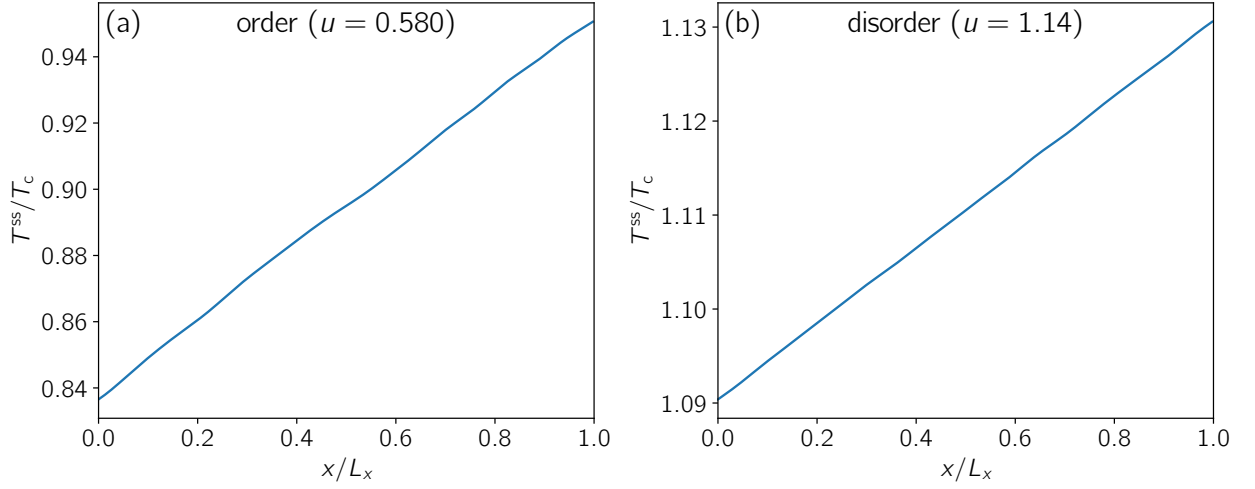


FIG. S.4. One dimensional temperature profile $T^{\text{ss}}(x)$ with $J = -0.00002$ starting from the initial conditions (S.56) with (a) $T = 0.9T_c$ (ordered phase with $u = 0.580$) and (b) $T = 1.1T_c$ (disordered phase with $u = 1.14$).

with setting $t_f = t_0 + 1.6 \times 10^4$.

D. Measurement of heat conductivity

To numerically evaluate θ^{Th} in (9), we have to know the values of heat conductivities κ° and κ^{d} in ordered and disordered states. We calculate them by solving the Hamiltonian equation (5) with the nonequilibrium boundary condition (8). Here, the initial condition is given by the final state of (S.71), that is,

$$(\phi, \pi_0)_{E,J}(x, y, 0) = \begin{cases} (\phi_1, \pi_1)_T(x, y, t = t_f) & 0 \leq x < L_x/2, \\ (\phi_2, \pi_2)_T(x - L_x/2, y, t = t_f) & L_x/2 \leq x < L_x, \\ (\phi_2, \pi_2)_T(0, y, t = t_f) & x = L_x. \end{cases} \quad (\text{S.56})$$

Note that the initial condition (S.56) is an equilibrium configuration at temperature T . That is, it is an ordered state when $T < T_c$ and a disordered state when $T > T_c$. We determine the local temperature profile $T^{\text{ss}}(x)$ by $\langle \hat{T}_x \rangle_{E,J}$ with (S.55).

For the calculation of κ° , we choose $T = 0.9T_c$ for the initial configuration (S.56). The corresponding energy density is $u = 0.580$, where the equilibrium system with energy fixed does not show phase coexistence. See Fig. S.2. As the value of u is sufficiently smaller than the saturation value $E_1/(L_x L_y)$, the local temperature $T^{\text{ss}}(x)$ is lower than T_c everywhere when applying the small constant heat flux $J = -0.00002$. See Fig. S.4 (a). The local temperature $T^{\text{ss}}(x)$ linearly increases from $x = 0$ to $x = L_x$, which supports that the value $J = -0.00002$ used in this work is so small for the system to be in the linear-response regime. We finally determine the heat conductivity by $\kappa^{\circ} = -JL_x/(T^{\text{ss}}(L_x) - T^{\text{ss}}(0))$.

For the calculation of κ^{d} , we choose $T = 1.1T_c$ for the initial configuration (S.56), where $u = 1.14$. As shown in Fig. S.4 (b), $T^{\text{ss}}(x)$ is higher than T_c everywhere in x with $J = -0.00002$, and therefore the nonequilibrium system is in the disordered state. The linear temperature profile confirms that the system is in the linear-response regime. We determine the heat conductivity as $\kappa^{\text{d}} = -JL_x/(T^{\text{ss}}_{E,J}(L_x) - T^{\text{ss}}_{E,J}(0))$.

Finally, we obtain $\kappa^{\circ} = 8.76JL_x/T_c$ and $\kappa^{\text{d}} = 24.8JL_x/T_c$. Using these values, we plot θ^{Th} in Fig. 4 (a).

E. Finite-size effect and roughness effect on the interface temperature

We separate the numerical data demonstrated in Fig. 4(b) of the main text to discuss effects of numerical parameters on the interface temperature in the heat conducting systems. Below, heat flux J is fixed to $J = -0.00002$.

Figure S.5 (a) shows the dependence of the interface temperature θ on the system size with the grid size $\Delta x = 1/8$ fixed. A comparison of the numerical results for $(L_x, L_y) = (384, 64)$, $(192, 32)$, and $(96, 16)$ clarifies the growth of the deviation of θ from T_c for larger system sizes. When performing numerical simulations in the smallest size $(96, 16)$, one

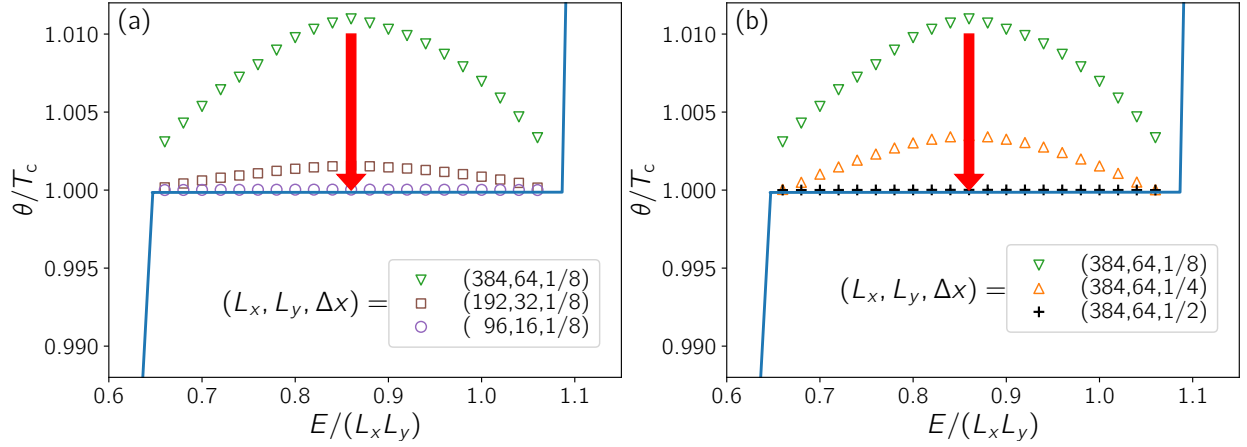


FIG. S.5. (a) Finite-size dependence of θ on $(L_x, L_y) = (384, 64)$, $(192, 32)$ and $(96, 16)$ with green inverted triangles, brown squares, and purple circles, respectively. The grid spacing $\Delta x = 1/8$ is fixed. (b) Roughness dependence of the θ on $\Delta x = 1/8$, $1/4$ and $1/2$ with green inverted triangles, orange triangles, and black crosses, respectively. The system size $(L_x, L_y) = (384, 64)$ is fixed. In both figures, the blue line indicates the equilibrium functional dependence between $E/(L_x L_y)$ and T obtained by the isothermal simulations explained in Sec. S III.

might conclude that the local equilibrium explains the heat conducting state well. Indeed, even the smallest system of $(96, 16)$ possesses 98,304 grid points, which may be thought as a large size in numerical simulations. However, our numerical results show that a much larger system size brings a qualitatively different behavior in heat conduction from smaller system sizes.

Next, we show in Fig. S.5 (b) the dependence on the grid size Δx with $(L_x, L_y) = (384, 64)$ fixed. The figure clearly shows that the interface temperature converges to T_c increasing the roughness of the system as $\Delta x = 1/8$, $1/4$ and $1/2$. The violation of the local equilibrium is hardly visible in $\Delta x = 1/2$. This fact implies that the violation of the local equilibrium requires not only the large system size but also regularity of fluctuations in a certain short wavelength.

III. DETERMINATION OF THE PHASE DIAGRAM IN FIG. 1 (B)

In this section, we figure out the calculation for determining the equilibrium phase diagram in Fig. 1 (b). We concentrate on the system at constant temperature T . The equilibrium state is described by the canonical ensemble

$$\rho_T^{\text{can}}(\phi, \pi) = \frac{1}{\mathcal{Z}} \exp(-\mathcal{H}(\phi, \pi)/T), \quad (\text{S.57})$$

where \mathcal{Z} is the normalization constant satisfying the condition

$$\int \mathcal{D}\phi \mathcal{D}\pi \rho_T^{\text{can}}(\phi, \pi) = 1. \quad (\text{S.58})$$

Since it is not easy to obtain the canonical ensemble in numerical simulations of the model that exhibits a first-order transition, we explain the numerical scheme we adopted.

A. Langevin equation and numerical methods

As an evolution equation consistent with the Hamiltonian equation (5), we adopt the Langevin equation

$$\partial_t \phi^a = \frac{\delta \mathcal{H}}{\delta \pi^a}, \quad \partial_t \pi^a = -\frac{\delta \mathcal{H}}{\delta \phi^a} - \gamma \pi^a + \xi^a, \quad (\text{S.59})$$

where $\xi^a(\mathbf{r}, t)$ is the white Gaussian noise satisfying

$$\langle \xi^a(\mathbf{r}, t) \xi^b(\mathbf{r}', t') \rangle = 2\gamma T \delta^{ab} \delta(\mathbf{r} - \mathbf{r}') \delta(t - t'). \quad (\text{S.60})$$

The canonical ensemble (S.57) is given as the stationary distribution of (S.59). We set $\gamma = 1$ without loss of generality.

We solve the Langevin equation (S.59) in a periodic box with $(L_x, L_y, \Delta x) = (192, 64, 1/8)$ consisting of $N_x \times N_y$ grid points with $(N_x, N_y) = (1536, 512)$ separated by the lattice spacing Δx . To calculate the spatial derivative $\nabla^2 \phi^a$ included in $\delta\mathcal{H}/\delta\phi^a$, we again use the spectral collocation method. There is a slight difference from (S.45) because of the difference of the boundary condition. Concretely, we use

$$\begin{aligned} \nabla^2 \Phi^a(x, y, t) &= -\frac{1}{N_x N_y} \sum_{n_x=-N_x/2+1}^{N_x/2} \sum_{n_y=-N_y/2+1}^{N_y/2} (k_x^2 + k_y^2) \tilde{\Phi}^a(n_x, n_y, t) e^{i(k_x x + k_y y)}, \\ k_x &= \frac{2\pi n_x}{L_x}, \quad k_y = \frac{2\pi n_y}{L_y}. \end{aligned} \quad (\text{S.61})$$

Note that \sum denotes the standard summation which is different from \sum' defined in (S.46). The Fourier component $\tilde{\Phi}^a(n_x, n_y, t)$ in (S.61) is obtained by the inverse-Fourier transformation

$$\tilde{\Phi}^a(n_x, n_y, t) = \sum_{I=0}^{N_x-1} \sum_{J=0}^{N_y-1} \Phi^a(x, y, t) e^{-i(k_x I + k_y J) \Delta x}. \quad (\text{S.62})$$

The $N_x \times N_y$ grid points evolve according to the Langevin equation (S.59). To obtain the time evolution of these points, we use the 2nd-order Strang splitting:

$$\begin{aligned} \phi^a(\mathbf{r}, t + \Delta t/2) &= \phi^a(\mathbf{r}, t) + \frac{\Delta t}{2} \pi^a(\mathbf{r}, t), \\ \pi^a(\mathbf{r}, t + \Delta t) &= \pi^a(\mathbf{r}, t) - \Delta t \left(\frac{\delta\mathcal{H}}{\delta\phi^a}(\mathbf{r}, t + \Delta t/2) + \pi^a(\mathbf{r}, t) \right) + \sqrt{2T(\Delta x)^2(\Delta t)} \Theta^a(\mathbf{r}, t), \\ \phi^a(\mathbf{r}, t + \Delta t) &= \phi^a(\mathbf{r}, t + \Delta t/2) + \frac{\Delta t}{2} \pi^a(\mathbf{r}, t + \Delta t), \end{aligned} \quad (\text{S.63})$$

where $\Delta t = 1/4096$ and $\Theta^a(\mathbf{x}, t)$ are the random numbers generated by the standard normal distribution. Below, we denote the solution of the Langevin equation (S.59) as $(\phi, \pi)_T(\mathbf{r}, t)$.

B. Metastable and equilibrium states

Compared with the Hamiltonian equation (5) investigated in Sec. II B, the Langevin equation (S.59) shows a faster relaxation because of no energy conservation. Since a typical relaxation time of the Langevin equation is independent of system sizes, it is four orders of magnitude shorter than that for the Hamiltonian equation where the relaxation time is proportional to L_x^2 . However, near the first-order transition, the system may relax to the metastable state rather than the equilibrium state. Once the system is trapped in the metastable state, it takes significant time to get out of it. Since the observed state depends on the initial condition, the system shows hysteresis.

Throughout the following sections, we fix the transient time as $t_0 = 1.0 \times 10^3$, and observe states from t_0 to $t_f = t_0 + 1.6 \times 10^4$. The time t_0 is much longer than the relaxation time to the equilibrium or metastable states, however, much shorter than the first passage time to get out of the metastable state. The observation period $t_f - t_0$ is so long that the finite time fluctuations can be ignored. In such a time scale, we cannot distinguish the metastable state from the equilibrium stats. Thus, we first examine the hysteresis and then proceed to the introduction of a numerical scheme for providing the canonical ensemble. Our aim is to determine the equilibrium energy density of the system

$$\bar{u}_T = \frac{1}{L_x L_y} \int \mathcal{D}\phi \mathcal{D}\pi \rho_T^{\text{can}}(\phi, \pi) \mathcal{H}(\phi, \pi), \quad (\text{S.64})$$

and the order parameter of the system

$$\bar{m}_T = \frac{1}{L_x L_y} \int_D d^2 \mathbf{r} \int \mathcal{D}\phi \mathcal{D}\pi \rho_T^{\text{can}}(\phi, \pi) \hat{m}(\mathbf{r}), \quad (\text{S.65})$$

which provides a phase diagram.

Below, we examine the equilibrium and metastable states over a wide range of T in $[T_{\min}, T_{\max}]$, where $T_{\min} = 0.0015$ and $T_{\max} = 0.3$. Precisely, we examine 201 temperature points,

$$T_k = T_{\min} + k\Delta T, \quad (k = 0, 1, \dots, 200), \quad (\text{S.66})$$

where $\Delta T \equiv (T_{\max} - T_{\min})/200$. Using the numerical data at various temperatures, we specify the equilibrium transition temperature T_c in Sec. III B 3. The results of the equilibrium simulations are shown in Figs. S.6 (a) and (b), where \bar{u}_T and \bar{m}_T exhibits the discontinuous jump at $T = T_c \simeq 0.150$. This indicates that the first-order transition occurs at $T = T_c$. Figure S.6 (a) is the same as that displayed in Fig. 1 (b).

1. Heating experiment

We start with the initial condition $(\phi, \pi)_{T_{\min}}(\mathbf{r}, 0) = (\mu_1, 0)$ at $T = T_{\min}$. Note that the direction of the symmetry breaking is specified by this initial condition in the following heating experiment. We numerically solve the Langevin equation (S.59) up to $t = t_f$ at $T_{\min} = T_{k=0}$, and calculate the time average of observables over the time interval $t_f - t_0$. That is, for

$$\bar{u}_{T_k}^{\text{heat}} \equiv \frac{1}{L_x L_y} \frac{1}{t_f - t_0} \int_{t_0}^{t_f} dt \mathcal{H}(\phi(t), \pi(t)), \quad (\text{S.67})$$

$$\bar{m}_{T_k}^{\text{heat}} \equiv \frac{1}{L_x L_y} \int_D d^2 \mathbf{r} \frac{1}{t_f - t_0} \int_{t_0}^{t_f} dt \hat{m}(\mathbf{r}, t), \quad (\text{S.68})$$

we obtain $(\bar{u}_{T_0}^{\text{heat}}, \bar{m}_{T_0}^{\text{heat}})$. We then increment the temperature from T_0 to T_1 and reset the time to be $t = 0$. The initial condition at $T = T_1$ is equal to the final state at T_0 , i.e., $(\phi, \pi)_{T_1}(\mathbf{r}, 0) = (\phi, \pi)_{T_0}(\mathbf{r}, t_f)$. We then numerically solve the Langevin equation (S.59) up to $t = t_f$. We repeat the same procedure changing the temperature from T_{k-1} to T_k and setting $(\phi, \pi)_{T_k}(\mathbf{r}, 0) = (\phi, \pi)_{T_{k-1}}(\mathbf{r}, t_f)$, where $1 \leq k \leq 200$. We plot the temperature dependence of $\bar{u}_{T_k}^{\text{heat}}$ and $\bar{m}_{T_k}^{\text{heat}}$ as displayed in Figs. S.6 (c) and (d). At $T \simeq 0.166$, the system suddenly enters the disordered state with $\bar{m}_T^{\text{heat}} \simeq 0$. At the same temperature, \bar{u}_T^{heat} also shows a discontinuous jump.

2. Cooling experiment

We start with an initial state which is obtained as the final state of the heating experiment. We then decrease the temperature from T_k to T_{k-1} , where k changes from $k = 200$ to $k = 1$. From each T_k , the time is reset as $t = 0$, and the initial condition at $T = T_{k-1}$ is $(\phi, \pi)_{T_{k-1}}(\mathbf{r}, 0) = (\phi, \pi)_{T_k}(\mathbf{r}, t_f)$ in the cooling experiment. Similarly to the heating experiment, we define

$$\bar{u}_{T_k}^{\text{cool}} \equiv \frac{1}{L_x L_y} \frac{1}{t_f - t_0} \int_{t_0}^{t_f} dt \mathcal{H}(\phi(t), \pi(t)), \quad (\text{S.69})$$

$$\bar{m}_{T_k}^{\text{cool}} \equiv \frac{1}{L_x L_y} \int_D d^2 \mathbf{r} \frac{1}{t_f - t_0} \int_{t_0}^{t_f} dt \hat{m}(\mathbf{r}, t). \quad (\text{S.70})$$

At a glance, (S.69) and (S.70) are the same as (S.67) and (S.68). The only but significant difference is the initial condition for each T_k . In the cooling experiment, we obtain Figs. S.6 (e) and (f). They are obviously different from Figs. S.6 (c) and (d). Through the cooling experiment, the system always shows the disordered state with $\bar{m}_T \simeq 0$ and the symmetry breaking never occurs, which suggests that the supercooled metastable disordered state can exist even close to the zero temperature. These results indicate the existence of a strong hysteresis in this system.

3. Equilibrium values

Now, we determine which quantity $(\bar{u}_T^{\text{heat}}, \bar{m}_T^{\text{heat}})$ or $(\bar{u}_T^{\text{cool}}, \bar{m}_T^{\text{cool}})$ corresponds to the equilibrium value. Here, we use the equilibration method developed by Ohzeki and Ichiki [5]. We consider a duplicated system comprising (ϕ_A, π_A) and (ϕ_B, π_B) , each of which is defined in the periodic box with $(L_x, L_y) = (192, 64)$. The duplicated system evolves

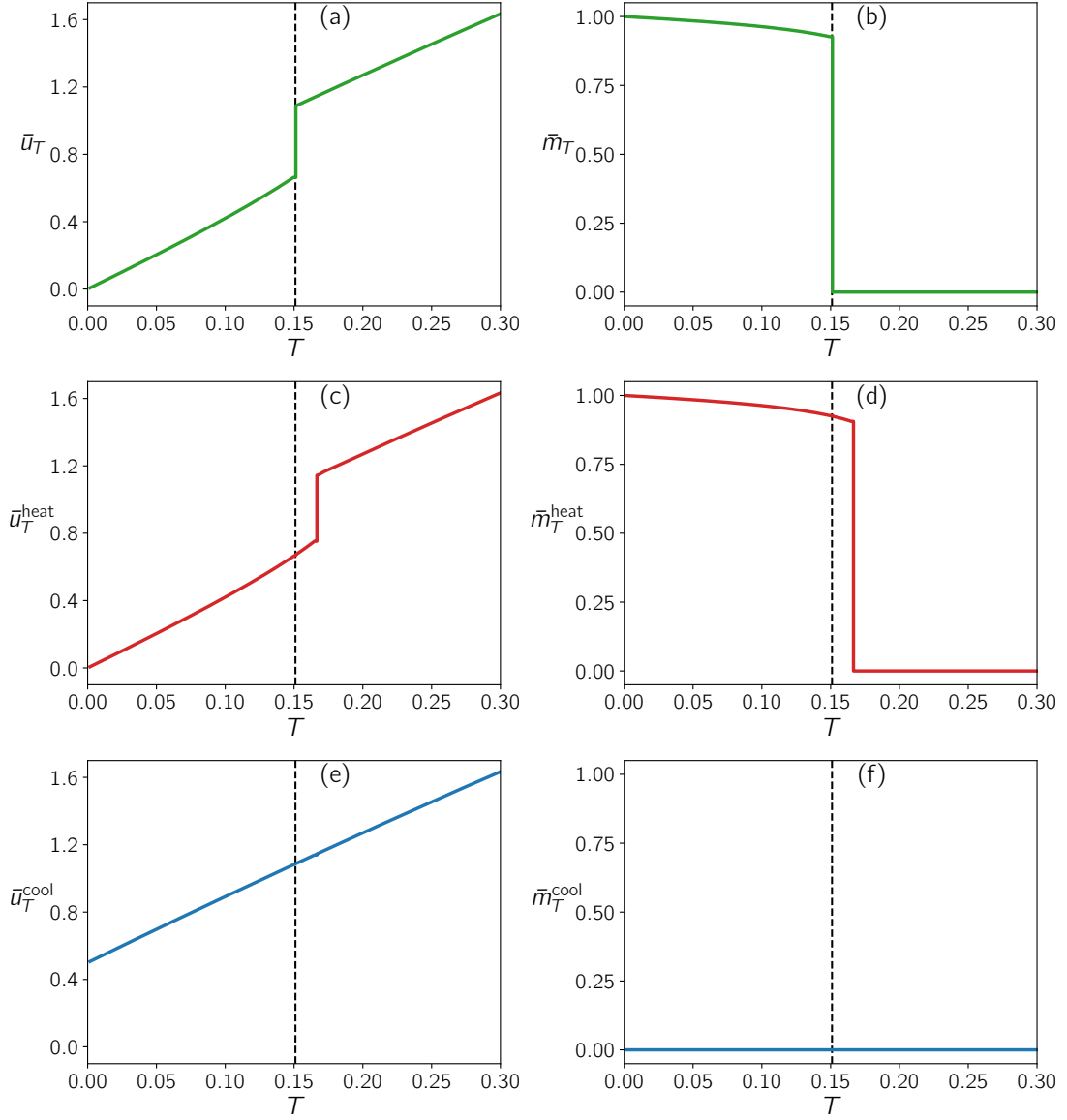


FIG. S.6. Temperature dependence of the energy density \bar{u}_T (panels (a), (c), and (e)) and the order parameter \bar{m}_T (panels (b), (d), and (f)) as the function of T for the equilibrium with the Langevin equation (S.71) (panels (a) and (b)), the heating experiment with the Langevin equation (S.59) (panels (c) and (d)), and the cooling experiment with the Langevin equation (S.59) (panels (e) and (f)).

by

$$\begin{aligned}
 \partial_t \phi_A^a &= \frac{\delta \mathcal{H}(\phi_A, \pi_A)}{\delta \pi_A^a} - \frac{\delta \mathcal{H}(\phi_B, \pi_B)}{\delta \pi_B^a}, & \partial_t \pi_A^a &= -\frac{\delta \mathcal{H}(\phi_A, \pi_A)}{\delta \phi_A^a} - \frac{\delta \mathcal{H}(\phi_B, \pi_B)}{\delta \phi_B^a} - \pi_A^a + \xi_A^a, \\
 \partial_t \phi_B^a &= \frac{\delta \mathcal{H}(\phi_B, \pi_B)}{\delta \pi_B^a} + \frac{\delta \mathcal{H}(\phi_A, \pi_A)}{\delta \pi_A^a}, & \partial_t \pi_B^a &= -\frac{\delta \mathcal{H}(\phi_B, \pi_B)}{\delta \phi_B^a} + \frac{\delta \mathcal{H}(\phi_A, \pi_A)}{\delta \phi_A^a} - \pi_B^a + \xi_B^a,
 \end{aligned} \tag{S.71}$$

where $\xi_i^a(\mathbf{r}, t)$ satisfies

$$\langle \xi_i^a(\mathbf{r}, t) \xi_j^b(\mathbf{r}', t') \rangle = 2\gamma T \delta^{ab} \delta_{ij} \delta(\mathbf{r} - \mathbf{r}') \delta(t - t'). \tag{S.72}$$

Writing down the Fokker-Planck equation, we can confirm that the stationary distribution of (S.71) coincides with the canonical distribution (S.57). It is also proved that the relaxation time of (S.71) to the true equilibrium is shorter than that of the original system (S.59) [5].

We solve (S.71) by discretizing the system with the lattice spacing $\Delta x = 1/8$ and using the same methods as those for the original Langevin equation (S.59). The initial condition at the temperature T is given as a couple of the final states obtained in the heating and cooling experiments,

$$(\phi_A, \pi_A)_T(\mathbf{r}, 0) = (\phi, \pi)_T(\mathbf{r}, t_f)^{\text{heat}}, \quad (\text{S.73})$$

$$(\phi_B, \pi_B)_T(\mathbf{r}, 0) = (\phi, \pi)_T(\mathbf{r}, t_f)^{\text{cool}}, \quad (\text{S.74})$$

where $(\phi, \pi)_T(\mathbf{r}, t_f)^{\text{heat}}$ and $(\phi, \pi)_T(\mathbf{r}, t_f)^{\text{cool}}$ are the final states at T calculated in Sec. III B 1 and Sec. III B 2, respectively. Let t_0 and t_f be the same value used in numerical simulations of the original Langevin equation (S.59). We observe that the subsystems A and B become to exhibit the same statistical state until $t = t_0$. We thus expect that the obtained states $(\phi_A, \pi_A)_T(\mathbf{r}, t)$ and $(\phi_B, \pi_B)_T(\mathbf{r}, t)$ for $t \geq t_0$ obey the respective canonical distribution $\rho_T^{\text{can}}(\phi_A, \pi_A)$ and $\rho_T^{\text{can}}(\phi_B, \pi_B)$ defined in (S.57). The equilibrium values \bar{u}_T and \bar{m}_T defined in (S.64) and (S.65) are then given by time averages in the interval $t_f - t_0$. Explicitly, we calculate them as

$$\bar{u}_T = \frac{1}{L_x L_y} \frac{1}{t_f - t_0} \int_{t_0}^{t_f} dt \frac{\mathcal{H}(\phi_A(t), \pi_A(t)) + \mathcal{H}(\phi_B(t), \pi_B(t))}{2}, \quad (\text{S.75})$$

$$\bar{m}_T = \frac{1}{L_x L_y} \int_D d^2 \mathbf{r} \frac{1}{t_f - t_0} \int_{t_0}^{t_f} dt \sum_{a=1}^{q-1} \frac{\phi_A^a(\mathbf{r}) + \phi_B^a(\mathbf{r})}{2} \mu_1^a. \quad (\text{S.76})$$

Since the duplicated system has (ϕ_A, π_A) and (ϕ_B, π_B) , we take the arithmetic means of the two in (S.75) and (S.76). Figures S.6 (a) and (b) show \bar{u}_T and \bar{m}_T obtained by (S.75) and (S.76), respectively.

In Fig. S.2, we also show the data of Fig. S.6 (a) in addition to the microcanonical temperature \bar{T}_E as a function of $u = E/(L_x L_y)$. The both data show quantitatively the same behavior including the states with the interface at $T = \bar{T}_E = \bar{T}_c$, which shows the equivalence of thermodynamic ensembles (S.50) and (S.57). This result also demonstrates the validity of the numerical method generating the canonical ensemble (S.57).

-
- [1] N. Nakagawa and S.-i. Sasa, Global thermodynamics for heat conduction states, *J. Stat. Phys.* **177**, 825-888 (2019).
 - [2] N. Nakagawa and S.-i. Sasa, Unique extension of the maximum entropy principle to phase coexistence in heat conduction, *Phys. Rev. Res.* **4**, 033155 (2022).
 - [3] B. Fornberg, *A practical Guide to Pseudospectral Methods*, Cambridge University Press (1995).
 - [4] R. I. McLachlan and G. R. W. Quispel, *Acta Numerica* **11**, 341 (2002).
 - [5] M. Ohzeki and A. Ichiki, Langevin dynamics neglecting detailed balance condition, *Phys. Rev. E* **92**, 012105 (2015).